Strong-field two-photon transition by phase shaping

Sangkyung Lee, Jongseok Lim, and Jaewook Ahn*
Department of Physics, Korea Advanced Institute of Science and Technology, Daejeon 305-701, Korea

Vahe Hakobyan and Stéphane Guérin
Laboratoire Interdisciplinaire Carnot de Bourgogne (ICB), Unité de Mixte de Recherche 5209 Centre National de la Recherche Scientifique-Université de Bourgogne, 9 Avenue A. Savary, Boîte Postale 47 870, F-21078 DIJON Cedex, France
(Received 17 February 2010; published 10 August 2010)

We demonstrate the ultrafast coherent control of a nonlinear two-photon absorption in a dynamically shifted energy level structure. We use a spectrotemporal laser-pulse shaping that is programed to preserve the resonant absorption condition during the intense laser-field interaction. Experiments carried out in the strong-field regime of two-photon absorption in the ground state of atomic cesium reveal that the analytically obtained offset and curvature of a laser spectrum compensate the effect of both static and dynamic energy shifts of the given light-atom interaction.

DOI: 10.1103/PhysRevA.82.023408 PACS number(s): 32.80.Rm, 42.50.Ct, 42.50.Hz, 42.65.Re

I. INTRODUCTION

Pulse-shape programming of ultrafast laser fields has enabled the development of many nonlinear light-matter interactions beyond simple transform-limited pulses [1]. By using a programed pulse shape, one can coherently control an atomic or molecular process by steering it through a desirable quantum path [2,3]. This novel concept of ultrafast coherent control has been applied to, for example, the optimization of nonlinear processes, such as multiphoton absorption, second- and third-harmonic generation, etc. [4–10]. In particular, ultrafast coherent control in multiphoton absorption has been studied widely in the weak-field regime where the energy level structure of the matter remains unchanged and population transfers are negligible [11–14]. There, the main goal is the laser spectral shaping to induce quantum interference among many near-degenerate quantum pathways for the given absorption process. However, a short laser pulse of ultrahigh peak intensity, although it enhances the nonlinear process, in general, can sometimes fail to optimize such an absorption process. This is due to light-induced energy level modifications, such as the power broadening and the dynamical Stark shift.

Even before the advent of ultrafast lasers, there were experiments performed with a two-photon absorption in atomic vapors in a strong-field regime, such as the coherent pulse breakup into subpulses [15]. In recent years, there have been many studies toward strong-field coherent control [16–22]. It is now well known that, in general, a control scheme devised in the weak-field regime cannot be directly applied to strong-field coherent control, although the partial information of the weak-field solution can still be useful [16]. There have been many approaches solely developed for strong-field coherent controls: the selective population of dressed states [17], the strong-field atomic phase matching [18], the phenomenological study of the symmetry breaking in spectrotemporal two-dimensional (2D) maps [19], the piecewise adiabatic passage [20], and the adiabatic Floquet theory [21]. Also, we have developed an analytical control approach in which the strong-field interaction is probed by laser pulses prepared in a polynomial sum of spectral phase terms [22].

In the strong-field regime where the structure of the energy levels is strongly altered during the pulse interaction, a more complicated ultrafast pulse design is required. One obvious strategy is to shape the laser pulse both in time and in frequency, in such a way that the absorption condition is maintained during the interaction (i.e., the laser frequency has to follow the energy difference of the concerned dressed states).

In this paper, we report an experimental demonstration of an optimal pulse shaping in which the static and dynamic energy level shifts are simultaneously compensated by a programed phase of a laser field. We perform analytical calculations, which guide the programming in a regime beyond perturbation theory where the Stark shifts and the population transfers are significant. In order to optimize the two-photon absorption in atomic cesium in the ground states, the frequency of the laser pulse is swept by following the temporal change of the absorption energy gap. In the case of a Gaussian pulse, it is shown that a temporal cubic phase is sufficient to retain the resonance condition during the interaction, since it very accurately allows one to recover the population transfer that would occur without Stark shifts.

The paper is organized as follows: In Sec. II, we describe the model and the pulse-shaping scheme. Section III is devoted to the experimental description. In Sec. IV, we present the results and their interpretation before concluding in Sec. V.

II. THEORETICAL CONSIDERATION

A. The model and the general phase-matching condition

For a two-state system that corresponds to a two-photon transition, the effective Hamiltonian in the resonant approximation can be written in the two-state basis $\{|g\rangle,|e\rangle\}$ (of respective energy ω_g,ω_e) as

$$H(t)=\hbar\begin{bmatrix}0 & \frac{1}{2}\Omega(t)\,e^{2i\phi(t)}\\ \frac{1}{2}\Omega(t)\,e^{-2i\phi(t)} & \Delta+\delta(t)\end{bmatrix}, \qquad (1)$$

where $\Omega(t)$ (chosen real) is the two-photon Rabi frequency and $\phi(t)$ is the phase of the laser field, relative to its mean

*jwahn@kaist.ac.kr

(or central) frequency ω_0. We have decomposed the detuning as $\Delta = \omega_e - \omega_g - 2\omega_0$, the static two-photon detuning, and $\delta(t)$ as the relative dynamical Stark shift. We have omitted irrelevant global phases. For a field amplitude of shape $\sqrt{\Lambda(t)}$, the Rabi frequency is of the form $\Omega(t) = \Omega_0\Lambda(t)$ with Ω_0 proportional to the peak-field intensity I_{peak}, and the Stark shift has the same time dependence: $\delta(t) = \delta_0\Lambda(t)$ with δ_0 also proportional to I_{peak}: $\delta_0 = r\Omega_0$ (see Appendix A for details). We consider Gaussian pulse shape $\Lambda(t) = \exp[-(t/\tau)^2]$.

The Hamiltonian can be written alternatively as $\hat{H} = \hat{T}^\dagger H \hat{T} - i\hbar\hat{T}^\dagger d\hat{T}/dt$,

$$\hat{H}(t) = \hbar \begin{bmatrix} 0 & \frac{1}{2}\Omega(t) \\ \frac{1}{2}\Omega(t) & \Delta + \delta(t) - 2\dot{\phi}(t) \end{bmatrix}, \tag{2}$$

in a representation $\Psi(t) = \hat{T}^\dagger\psi(t)$ of the original state $\psi(t)$ associated with the diagonal transformation (which leaves the population unchanged) $\hat{T}(t) = |g\rangle\langle g| + e^{-i2\phi(t)}|e\rangle\langle e|$.

It is known (see, for instance, Ref. [23] for a proof, which uses the geometric control theory and Ref. [18] for an experimental demonstration through a learning algorithm) that, for such a two-state Hamiltonian Eq. (2), the minimum pulse area of the Rabi frequency to achieve the complete transfer is $\int dt\,\Omega(t) = \pi$ and that it is achieved when the exact resonance is satisfied at each time:

$$2\dot{\phi}(t) = \Delta + \delta(t). \tag{3}$$

This phase-matching condition can be interpreted as a compensation of the dynamical Stark shifts by the shaping of the pulse to maximize the resonance effects. No additional chirping of the field can decrease the π-pulse area. This result, Eq. (3), can be derived within the lowest order of the perturbation theory [24], which leads, for the probability of population transfer, to the excited state,

$$P_e(t) \approx \frac{1}{4}\left|\int_{t_i}^{t} dt'\,\Omega(t')\,e^{-i[2\phi(t')-\Delta t'-\int^{t'}\delta(u)\,du]}\right|^2, \tag{4}$$

where the error is of order $O(\epsilon^3)$ with respect to half of the partial area of the Rabi frequency: $\epsilon(t) \equiv \int_{t_i}^{t} dt'\,\Omega(t')/2$. Here, t_i indicates the initial time of the interaction. However, the phase-matching condition Eq. (3) is valid beyond the perturbation theory as long as the two-state model Eq. (2) is preserved.

It is of interest to determine general analytic pulse-shaping programming to satisfy this phase-matching condition [22]. In the following, we derive and test approximate conditions with simple pulse shapes, which compensate the dynamical Stark shifts, in order to lead to an efficient population transfer.

B. Optimal phase-matching condition near the peak value of the Stark shift

We perform a series expansion of the dynamical Stark shift and of the phase in the time domain to satisfy the phase-matching condition near its maximum in absolute value (i.e., around $t = 0$). By truncating the series by keeping the cubic terms, we get a transfer probability proportional to the peak intensity of the field,

$$P_e(\eta,\theta,\xi) \propto \left|\int_{-\infty}^{\infty} e^{-X^2+i\eta X+i\theta X^2+i\xi X^3}\,dX\right|^2, \tag{5}$$

where the dimensionless control parameters are defined as $\eta = 2\dot{\phi}(0)\tau - (\delta_0+\Delta)\tau$, $\theta = \ddot{\phi}(0)\tau^2$, and $\xi = [\dddot{\phi}(0)\tau^3 + \delta_0\tau]/3$. We determine the optimal pulse shape from the maximum value of Eq. (5), which corresponds to $\eta = \theta = \xi = 0$. This leads to nonzero linear and cubic phase terms and a zero quadratic phase:

$$2\phi(t) = (\Delta+\delta_0)t - \frac{1}{3}\frac{\delta_0}{\tau^2}t^3. \tag{6}$$

Figure 1(a) shows the probability of strong-field TPE from Eq. (5). The point O in Fig. 1(a) corresponds to the unshaped transform-limited pulse, and O_p corresponds to the optimal pulse shape ($\eta = \xi = 0$). The spectrotemporal shape at O_p can be illustrated as in Fig. 1(e). The control parameters $\dot{\phi}(0)$ in η

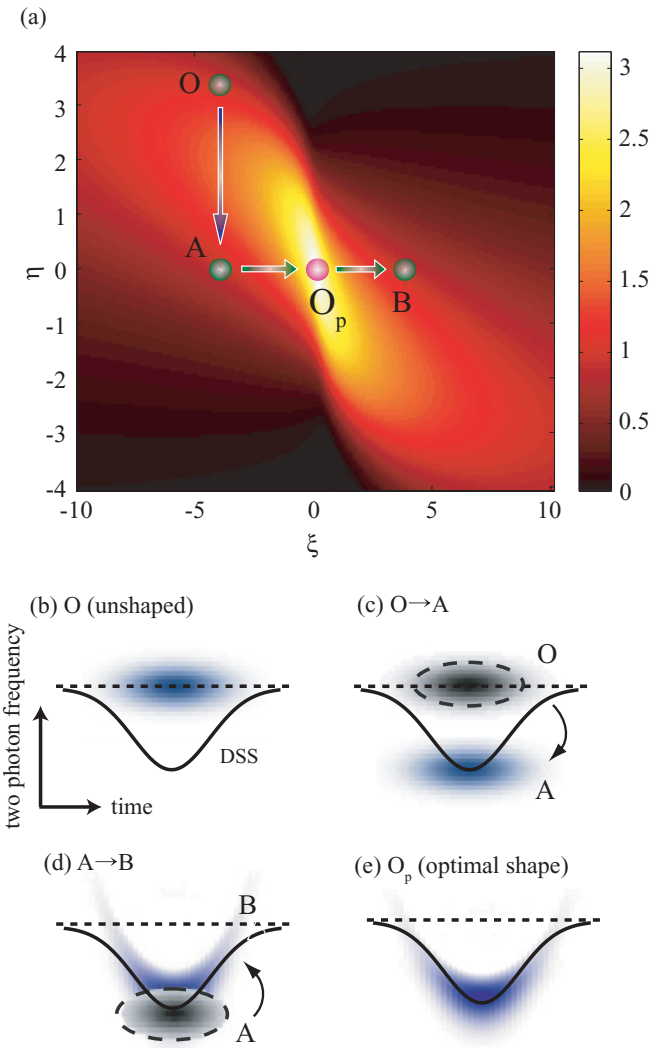

FIG. 1. (Color online) (a) Strong-field two-photon excitation (TPE) probability $P_e(\eta,\xi)$ (arb. units) calculated as a function of dimensionless parameters: the frequency detuning η and the spectral curvature ξ. (b) Two-photon spectrogram (as shaded contour plot, see Appendix B) of the unshaped pulse at the point $O(\delta_0\tau/3, -\Delta\tau - \delta_0\tau)$, where Δ and δ_0 denote the static and peak dynamic level shifts, respectively. The (negative) dynamic level shift is drawn as a full line. (c) Control of the detuning along $\overline{OA}$. (d) Spectral curvature control along $\overline{AB}$. (e) Two-photon spectrogram of the optimally shaped pulse at the point $O_p(0,0)$.

and $\dddot{\phi}(0)$ in ξ denote the frequency offset (detuning) and the frequency curvature in a spectrogram, respectively. Therefore, the change of η along the path $\overline{OA}$ in Fig. 1(a) is the frequency detuning as illustrated in Fig. 1(c). Also, the change of ξ along $\overline{AB}$ is the frequency curvature control as shown in Fig. 1(d).

III. EXPERIMENTAL DESCRIPTION

For the experiment, we used subpicosecond infrared pulses with a pulse energy of up to 100 μJ produced from a Ti:sapphire laser amplifier system, which operates at a repetition rate of 1 kHz. The pulses were shaped by an acousto-optic programmable dispersive filter (DAZZLER) and were illuminated on cesium atoms (^{133}Cs) of a gas density of 2.2×10^{16} m^{-3} in an optical cell at room temperature. The laser frequency was tuned to make the two-photon resonant condition for the $6S_{1/2}$-$8S_{1/2}$ transition at the low laser intensity limit, which implies $\delta \approx 0$ (i.e., $\Delta = 0$). The laser peak intensity (at the focus) was varied in the range of $0 \sim 0.2I_0$ ($I_0 = 10^{11}$ W/cm^2). We remark that intensities above this range start to produce a significant ionization from the upper state (see Appendix A for details of the model, which include the ionization rate from the upper state). Then, the atoms in the excited $8S_{1/2}$ state decay first to the $7P_{1/2}$ state and then down to the $6S_{1/2}$ ground state. We used the $7P_{1/2}$-$6S_{1/2}$ fluorescence signal collected by a photomultiplier tube to estimate the excitation probability of the $6S_{1/2}$-$8S_{1/2}$ transition. The collision coherent time and the transit time (average escape time of atoms that pass the beam diameter) are 66 and 390 ns, and the the lifetime of $8S_{1/2}$ is 90 ns [25].

The field, before its spectral shaping, is of Gaussian shape with the mean frequency ω_0: $\mathcal{E}_{\rm in}(t) = \mathcal{E}_{0\rm in} e^{-(t/\tau_{\rm in})^2} e^{i\omega_0 t}$. The programming target pulse $\mathcal{E}(t)$ also is chosen to be of Gaussian shape:

$$\mathcal{E}(t) = \mathcal{E}_0\, e^{-(t/\tau)^2} e^{i[\omega_0 t + \phi(t)]}. \tag{7}$$

The shaping in the frequency domain is such that

$$\widetilde{\mathcal{E}}(\omega) = A(\omega)\, e^{i\phi(\omega)} \widetilde{\mathcal{E}}_{\rm in}(\omega), \tag{8}$$

where $0 \leqslant A(\omega) \leqslant 1$ is the transparency coefficient of the shaping device, $\phi(\omega)$ is the spectral phase, and $\widetilde{F}(\omega) = \frac{1}{2\pi}\int_{-\infty}^{+\infty} F(t)\, e^{-i\omega t}\, dt$ denotes the Fourier transform. The pulse shaper is capable of tailoring both amplitude $A(\omega)$ and phase $\phi(\omega)$ in the frequency domain.

The laser beam focused onto the atoms has a spatial intensity profile,

$$I(r,z) = I_{\rm peak} \frac{w_0^2}{w^2(z)}\, e^{-r^2/w^2(z)}, \tag{9}$$

where $w(z)$ is the beam waist. As a result, we have determined numerically that the averaged field intensity and, consequently, the averaged dynamic Stark shift are approximately reduced by a factor 2 with respect to a uniform intensity profile. The calculated averaged dynamic Stark shift is roughly $\delta_0 = -10 \times 10^{12}$ rad/s (or -10 Trad/s) at $I_{\rm peak} = 20$ GW/cm^2 (see Appendix A for a more detailed discussion about the modeling of the driven cesium atoms).

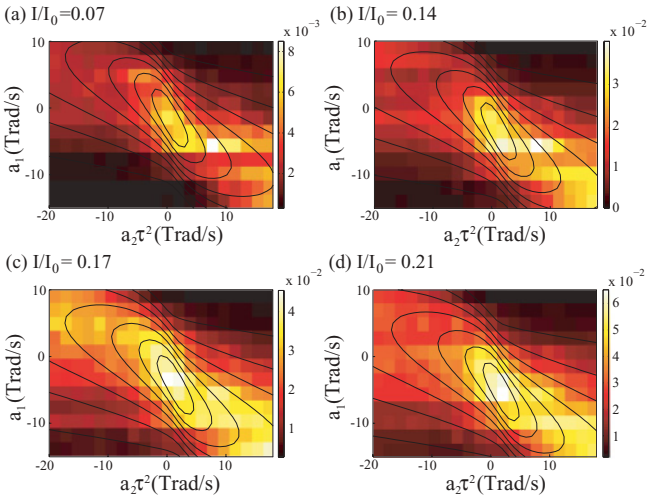

FIG. 2. (Color online) Fluorescence 2D maps measured at laser peak intensities $I_{\rm peak}/I_0 = 0.06$, 0.14, 0.17, and 0.21, as a function of a_1 and $a_2\tau^2$ parameters. Contour lines are calculated by using Eq. (5).

IV. RESULTS AND DISCUSSION

A. Verification of the optimal pulse shaping

The verification of the optimal pulse-shaping scheme discussed in Sec. II is carried out by measuring the $7P_{1/2}$-$6S_{1/2}$ fluorescence as a function of the phase $\phi(t)$ defined in Eq. (7). The result is shown in Fig. 2, where $\phi(t)$ is programed as a function of the coefficients a_1 and a_2, which define the variations of the cubic phase:

$$\phi(t) = a_1 t + a_2 t^3. \tag{10}$$

In our experiment, we use peak intensities such that $I_{\rm peak} \lesssim 0.2I_0$ and fields of duration $\tau = 90$ fs (that correspond to an intensity time profile of full width at half maximum 150 fs). A field of peak intensity $I_{\rm peak} = 0.47I_0 = 47$ GW/cm^2 leads to a complete population transfer (at the focus). We have checked from numerics that one can use Eq. (4) to determine the line shapes (and contour lines) in a rather good approximation. Moreover, the use of Eq. (5) instead of Eq. (4) to fit our experiments does not show a significant difference. The experiment does not allow us to very accurately determine the optimal value of a_2.

Along the vertical lines in Fig. 1(a), the frequency detuning experiments are shown in Fig. 3, compared with the numerical calculations. Figure 3(a) shows the line shapes of the signal, measured at the three different laser peak intensities, as functions of the frequency offset a_1 at zero cubic phase (i.e., $a_2 = 0$). The maximum of the signal is found at a larger frequency offset for a larger $I_{\rm peak}$. A more careful analysis shows that a_1 is proportional to $I_{\rm peak}$ as predicted in Sec. II [see Eq. (6)].

Also, the signal is measured as a function of the frequency curvature $a_2\tau^2$ at zero linear phase (i.e., $a_1 = 0$). As shown in Fig. 3(b), the signal is measured with zero detuning (i.e., $a_1 = 0$) as a function of the frequency curvature $a_2\tau^2$. The line shape is symmetric at a low intensity (the lowest red line) but becomes gradually asymmetric at higher intensities [the black (middle) and blue (upper) lines]. As the peak intensity

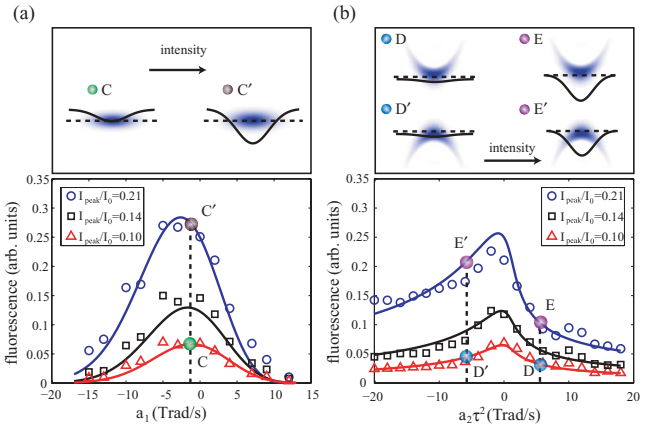

FIG. 3. (Color online) Strong-field TPE of cesium studied at three different laser intensities $I_{\text{peak}}/I_0 = 0.21,\ 0.14,\ 0.10$. The theoretical lines from Eq. (5) are compared with the $7P_{1/2}$-$6S_{1/2}$ fluorescence signal measured (a) as a function of the frequency offset a_1, defined in Eq. (10), at zero-frequency curvature $a_2 = 0$; and (b) as a function of the frequency curvature $a_2\tau^2$ at zero-frequency offset $a_1 = 0$. The upper panels show the two-photon spectrograms (shaded contour plots, see Appendix B) overlapped with the corresponding dynamically shifted energy levels (solid lines). The dotted lines represent the center frequency ω_0 of the shaped pulse.

increases, the overlap between the shifted energy level and the laser spectral distribution gradually decreases. As a result, the TPE in cesium at zero-frequency offset is better achieved by a negative cubic phase term. This seems counterintuitive because the curvature of the laser spectral distribution is opposite that of the shifted energy level. However, as illustrated in the top panel of Fig. 3(b), the pulse at E' with a negative cubic phase makes a better overlap with the detuned energy level than the pulse at E with a positive cubic phase. Therefore, the TPE rate in cesium at zero-frequency offset is higher with a negative quadratic frequency chirp.

Figure 4 shows the pulse-shape dependence of the TPE in cesium. For a simple detuning experiment ($a_2 = 0$), shown by

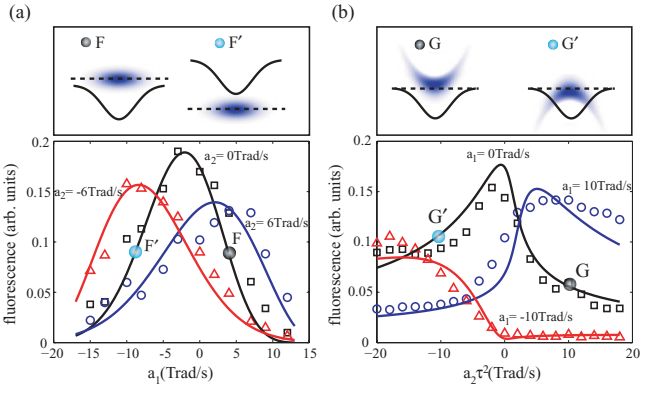

FIG. 4. (Color online) Pulse-shape dependence of TPE in cesium: The excitation is measured (a) as a function of frequency offset a_1 at fixed frequency curvatures $a_2 = 0$, 6, and -6 Trad/s, respectively; and (b) as a function of frequency curvature $a_2\tau^2$ at fixed frequency offsets $a_1 = 0$, 10, and -10 Trad/s, respectively. The peak intensity of the laser pulse is maintained at $I_{\text{peak}} = 1.7 \times 10^{10}$ W/cm^2. Upper panels: as in Fig. 3.

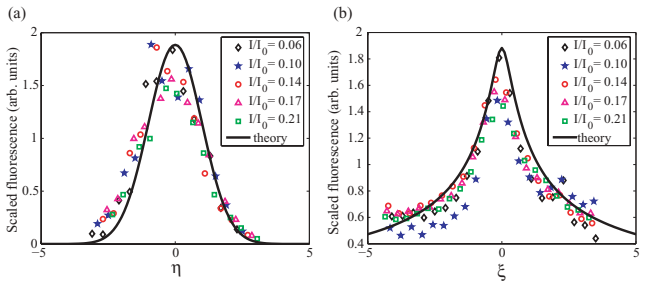

FIG. 5. (Color online) Scaled strong-field two-photon absorption profile $P_e/I^2\tau^2$ in Eq. (5) is plotted as a function of (a) $\eta = (2a_1 - \delta_0)\tau$ and (b) $\xi = 2a_2\tau^3 + \delta_0\tau/3$.

the black line (with open squares) in Fig. 4(a), the excitation maximum is found at a negative a_1, since $\delta_0 < 0$. We note that the optimal point for the intensity $I_{\text{peak}} = 1.7 \times 10^{10}$ W/cm^2 is located at $a_1 = -4.25$ Trad/s and $a_2\tau^2 = 1.4$ Trad/s from the analysis of Sec. II. The curvature control experiments shown in Fig. 4(b) are along the horizontal lines in Fig. 1(a). The measured signals are of more complex line shapes: Near the optimal detuning at $a_1 = 0$ [black line (with open squares)], as the curvature a_2 increases, the signal gradually grows and rapidly increases near $a_2 = 0$ (near O_p). For a more (less) detuned case with the positive (negative) a_1 in the blue (with open circles) [red (with open triangles)] line, the signal rapidly decreases (increases) near $a_2 = 0$.

Finally, from Eq. (5), the intensity invariant forms of excitation probability can be calculated as a function of each single parameter η and ξ, respectively,

$$P_e(\eta,0,0) = \sqrt{\pi}e^{-\eta^2/2}, \tag{11}$$

$$P_e(0,0,\xi) = \sum_{k=0}^{\infty}(-1)^k\xi^{2k}\frac{\Gamma(3k+1/2)}{(2k)!}. \tag{12}$$

They are drawn in Fig. 5 overlaid with the measured data points from Fig. 2. We note that the overall probabilities of strong-field two-photon transition $P_e/I^2\tau^2$ follow the theoretically obtained intensity invariant forms from Eq. (5).

B. Further optimization of the phase-matching condition

One can further improve the approximate condition Eq. (6) by determining conditions that allow one to recover the population transfer that would be obtained without Stark shifts. To that end, we determine the population transfer to the excited state at the end of the process, from the numerical integration of the Schrödinger equation, for various (strong or not) peak-field amplitudes and Stark shifts by using a phase of the form Eq. (10). Here, we do not consider the spatial averaging. We first make the analysis by using the two-state model Eq. (2). This is extended in Sec. IV C to a more accurate model of cesium for strong fields. Figure 6 shows two typical contour plots of the deviation from the population transfer to the excited state achieved without Stark shifts, with a pulse area of (a) π and (b) $\pi/2$, which correspond to a population transfer without Stark shifts of 1 and 0.5, respectively. We obtain (by taking $\Delta = 0$) the approximate optimal function that allows one to

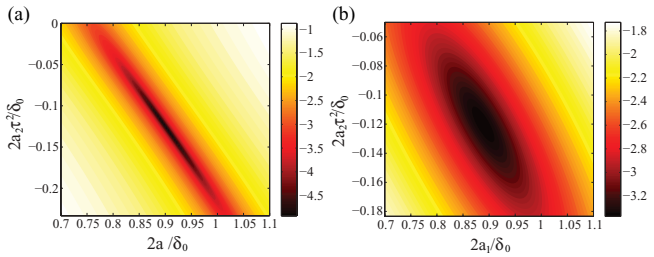

FIG. 6. (Color online) Contour plot (in the logarithmic scale to base 10) at the end of the pulse of the deviation from the population transfer in the absence of Stark shifts as a function of the dimensionless quantities $2a_1/\delta_0$ and $2a_2\tau^2/\delta_0$ for $\Delta = 0$, $\delta_0 = \Omega_0$, and (a) $\tau\Omega_0 = \sqrt{\pi}$ and (b) $\tau\Omega_0 = \sqrt{\pi}/2$. They correspond to complete and half population transfers, respectively, in the absence of Stark shifts.

accurately recover the population transfer without Stark shifts:

$$2\phi(t) = \delta_0\left(0.89t - 0.12\frac{t^3}{\tau^2}\right). \tag{13}$$

This has been obtained for a field intensity not larger than the one that leads to a complete population transfer in the absence of Stark shifts.

The demonstration of the exact optimal values of the linear and cubic terms in Eq. (13) is found to be beyond the scope of the accuracy of the present experiments. However, it is remarkable that this optimized function is a simple linear function of the peak Stark shift and, thus, of the peak-field amplitude, as anticipated in the preceding analysis. The value obtained for the linear term is close to the one determined with the truncated expansion Eq. (6). We have checked that the perturbation theory Eq. (4) gives a good approximation for the population transfer until the transfer of approximately 0.15 (error of 5%), which corresponds to a pulse area approximately of 0.25π (consistent with the estimated error of the perturbative expansion). Despite this limitation, we have obtained the interesting result that the line shapes can be approximately well described, up to a scaling factor (which depends on the intensity and the Stark shifts and that has to be determined with the numerical simulation), by the perturbation theory, even for stronger-field intensities.

C. Optimized phase matching beyond the two-state model for cesium

For the population transfer in cesium atoms between states $6S_{1/2}$-$8S_{1/2}$, a two-state approximation is, in principle, valid for intensities not larger than approximately 10 GW/cm^2 (see Appendix A for a precise statement). By using the four-state Hamiltonian Eq. (A11) derived in Appendix A, we numerically derive conditions of cubic phase matching to get the best population transfer at the lowest possible field intensity. The lowest field intensity has been found to be $I = 47$ GW/cm^2 with the cubic phase:

$$2\phi(t) = \delta_0\left(0.75t - 0.10\frac{t^3}{\tau^2}\right). \tag{14}$$

We get a population transfer of 99%, and the rest is ionized. We remark that the use of only a linear phase already allows a good transfer (98%). We notice that, for increasing intensities, by deviating from the two-state model, the optimal cubic phase moves to smallest values in absolute values for the linear and cubic terms. We have obtained numerically that the coefficients after the spatial averaging saturates to $a_1 \approx -4.5$ Trad/s and $a_2\tau^2 \approx 0.5$ Trad/s for fields intensities beyond 20 GW/cm^2 in consistency with the experimental results.

D. Strong-field TPE in other alkali-metal atoms

The TPE in cesium is characterized as nonresonant for a sufficiently low-field intensity, which means that no intermediate states are directly involved (see Appendix A for the precise conditions of this statement). The dynamic Stark shift of the $6S_{1/2}$ state is mainly determined by its coupling with the $6P_{1/2}$ and $6P_{3/2}$ states. The other couplings lead to a ponderomotive shift, which is much smaller [26]. The $6S_{1/2}$ state is upshifted by the dynamic Stark effect due to its repulsion with the two dressed states $|6P_{1/2}, -1\rangle$ and $|6P_{3/2}, -1\rangle$. The shift of $8S_{1/2}$ is due to its coupling mainly with the P states and weakly with the continuum. The net dynamic shift between $6S_{1/2}$-$8S_{1/2}$ is negative (see Appendix A).

On the other hand, TPE in rubidium or in sodium features an additional single-photon resonance. A typical femtosecond laser pulse of the center wavelength at 778 nm, that, in principle, allows TPE in rubidium between states $5S_{1/2}$ and $5D_{3/2,5/2}$, indeed strongly induces population into the intermediate nearly resonant state $5P_{3/2}$ [27]. Thus, the TPE in rubidium should be described by a three-level model $5S_{1/2}$-$5P_{3/2}$-$5D_{3/2,5/2}$ even for moderate-field intensities. Note that $5P_{1/2}$ can also be populated for strong fields. In sodium, a laser pulse of center wavelength 777 nm induces the $3S_{1/2}$-$4S_{1/2}$ TPE process but also a $4S_{1/2}$-$7P_{1/2}$ single-photon process [24]. Therefore, TPE in sodium should be modeled by a three-level system, similar to the case of rubidium. In both cases, the detuning that corresponds to the one-photon resonance is 1 order of magnitude smaller than the one in cesium from $6S_{1/2}$ and $6P_{3/2}$.

V. CONCLUSION

In conclusion, we theoretically analyzed and experimentally demonstrated the optimization scheme for the two-photon two-level system in the strong-field regime. By analyzing the optimal pulse shaping for the given TPE by using an effective two-state model, we have analytically obtained the optimal solution, which is to maintain the two-photon resonance condition nearly zero during the atom-light combined Hamiltonian. The resonance excitation condition is well maintained during the light-matter interaction by the linear and cubic temporal phase terms.

ACKNOWLEDGMENTS

This research was supported by Basic Science Research Program through the National Research Foundation of Korea (NRF) funded by the Ministry of Education, Science and Technology (Grant No. 2009-0090843). V.H. and S.G. acknowledge support from the Marie Curie Initial Training Network Grant No. CA-ITN-214962-FASTQUAST and the

French Agence Nationale de la Recherche (Project No. CoMoC). We thank Y. Kalugina for providing computing help.

APPENDIX A: MODEL FOR THE CESIUM ATOM DRIVEN BY A TWO-PHOTON PROCESS

A. The two-state approximation for a two-photon transition

1. Definition

The effective Hamiltonian for a two-photon transition between two states of respective energies ω_g and ω_e by a laser of phase $\varphi(t) = \omega_0 t + \phi(t)$ (with ω_0 as its mean frequency), which corresponds to the instantaneous (or effective) laser frequency $\omega_L(t) \equiv \dot{\varphi}(t) = \omega_0 + \dot{\phi}(t)$, reads in the resonant approximation:

$$H_2(t) = \hbar \begin{bmatrix} \omega_g + S_g(t) & \frac{1}{2}\Omega(t)e^{2i\varphi(t)} \\ \frac{1}{2}\Omega(t)e^{-2i\varphi(t)} & \omega_e + S_e(t) - i\frac{1}{2}\Gamma_e(t) \end{bmatrix}. \quad \text{(A1)}$$

The Stark shifts $S_g(t)$ and $S_e(t)$, respectively, of the ground and excited states, are due to their coupling to the intermediate states m and the continuum channels ℓ,

$$S_j(t) = -\frac{\mathcal{E}^2(t)}{2\hbar^2}\left[\sum_{m\neq j} |\mu_{jm}|^2 \frac{\omega_{mj}}{\omega_{mj}^2 - \omega_L^2(t)} + \mathrm{P}\int \frac{dE}{\hbar}\sum_{\ell} |\mu_{j;E,\ell}|^2 \frac{\omega_{Ej}}{\omega_{Ej}^2 - \omega_L^2(t)}\right], \quad \text{(A2)}$$

with $j = e,g$, μ_{jm} (respectively, $\mu_{j;E,\ell}$) the transition dipole moments between the state j, of energy $\hbar\omega_j$, and the intermediate state (respectively, the continuum state of the channel ℓ and of energy E), and $\omega_{mj} = \omega_m - \omega_j$, $\omega_{Ej} = E/\hbar - \omega_j$. P indicates the principal part of the integral when it is indefinite (if $\omega_j + \omega_L$ reaches the continuum). The effective two-photon Rabi frequency between the ground and the excited states is

$$\Omega(t) = -\frac{\mathcal{E}^2(t)}{2\hbar^2}\left[\sum_{m\neq e,g} \frac{\mu_{gm}\mu_{me}}{\omega_m - \omega_g - \omega_L(t)} + \int \frac{dE}{\hbar}\sum_{\ell} \frac{\mu_{g;E,\ell}\mu_{E,\ell;e}}{E/\hbar - \omega_g - \omega_L(t)}\right]. \quad \text{(A3)}$$

The field intensity $I(t)$ is related to the field amplitude $\mathcal{E}(t)$ through the relation $I\ [\mathrm{W/cm^2}] \approx 3.51 \times 10^{16}\,(\mathcal{E}[\mathrm{a.u.}])^2$. It is usually a good approximation to consider the mean (or central) frequency of the laser ω_0 instead of the instantaneous one $\omega_L(t)$ to calculate the Stark shifts and the Rabi frequency. This is generally the case when the frequency of the laser is chirped on a very small interval $\Delta\omega_L \equiv \Delta\dot{\phi} \ll \omega_0$. In that case, one has a constant ratio r between the relative Stark shift $\delta(t)$ and the two-photon Rabi frequency:

$$\delta(t) \equiv S_e(t) - S_g(t) = r\Omega(t). \quad \text{(A4)}$$

One has also considered that the excited state is lossy through ionization by the laser. This is taken into account by summing the partial rates to the continuum channel ℓ:

$$\Gamma_e(t) = \sum_{\ell} \Gamma_e^{(\ell)}, \quad \Gamma_e^{(\ell)} = \frac{\pi}{2\hbar}\mathcal{E}^2(t)|\mu_{e;E=\hbar\omega_e+\hbar\omega_L,\ell}|^2. \quad \text{(A5)}$$

Here, the partial rates have been written for the case of a single photon resonant in the continuum from the excited state.

2. Condition of validity

This resonant two-state approximation is valid when, for all $m \neq g,e$ and $j = g,e$,

$$|\Omega_{jm}| \ll |\Delta_{jm}|, \quad \text{(A6a)}$$

$$|\Omega_{jm}|, |\omega_e - \omega_g - 2\omega_L| \ll \omega_L, \quad \text{(A6b)}$$

with the one-photon detunings defined as

$$\Delta_{gm} = \omega_m - \omega_g - \omega_L, \quad \Delta_{em} = -\omega_m + \omega_e - \omega_L, \quad \text{(A7)}$$

which correspond to the one-photon Rabi frequencies:

$$\Omega_{jm} = -\mu_{jm}\mathcal{E}/\hbar. \quad \text{(A8)}$$

B. The two-photon $6S_{1/2}$-$8S_{1/2}$ transition in cesium

We consider the two-photon transition in cesium between the state $g \equiv 6S_{1/2}$ and $e \equiv 8S_{1/2}$. The mean frequency ω_0 of the laser [which corresponds to the laser frequency of the Fourier-transform pulse (i.e., before its shaping)] is exactly two-photon resonant: $\omega_0 = (\omega_g - \omega_e)/2$ (i.e., $\Delta = 0$). The relevant parameters for the considered transition are given in Table I. We have determined the parameters that involve the dipole moment couplings with Eqs. (A2), (A3), and (A5) by using Ref. [28] for the bound-bound couplings and the Fues model potential [29,30] for the bound-free couplings (see also Ref. [31] for a general discussion of model potential methods).

A single photon allows the ionization of the atom from the excited state, however, through the small ratio $|\Gamma_e/\Omega| = 6.5 \times 10^{-3}$.

Two intermediate states ($1 \equiv 6P_{1/2}$ and $2 \equiv 6P_{3/2}$, of respective energy ω_1 and ω_2) are close to a single-photon resonance and lead to strong Stark shifts in the effective two-state model Eq. (A1). Here, we derive the conditions of validity for this two-state model. The static one-photon detunings are

$$\Delta_{g1} \equiv \omega_1 - \omega_g - \omega_0 = -4.47 \times 10^{-3}\ \text{a.u.}, \quad \text{(A9)}$$

$$\Delta_{g2} \equiv \omega_2 - \omega_g - \omega_0 = -1.94 \times 10^{-3}\ \text{a.u.} \quad \text{(A10)}$$

For a laser intensity $I = 10\,\mathrm{GW/cm^2}$, we get for the peak single-photon Rabi frequencies (in a.u.) $\Omega_{g1} = 10^{-3} <$

TABLE I. Parameters for the transition in cesium $6S_{1/2}$-$8S_{1/2}$.

r	$\omega_e - \omega_g$ (rad/s)	ω_0 (rad/s)
1.85	4.58×10^{15}	2.29×10^{15}
$S_e - S_g$ (rad/ps)	Ω (rad/ps)	Γ_e (rad/ps)
$-1.0I$ (GW/cm^2)	$-0.54I$ (GW/cm^2)	$3.5 \times 10^{-3}I$ (GW/cm^2)

$|\Delta_{g1}|$ and $\Omega_{g2} = 1.4 \times 10^{-3} \sim |\Delta_{g2}|$, which, in principle, prevents the use of a two-state approximation. For intensities beyond $I = 10\ \mathrm{GW/cm^2}$, we, thus, use a four-level approximation:

$$H_4(t) = \hbar \begin{bmatrix} S_g(t) & \frac{1}{2}\Omega_{g1}(t) & \frac{1}{2}\Omega_{g2}(t) & \frac{1}{2}\Omega_{ge}(t) \\ \frac{1}{2}\Omega_{g1}(t) & \Delta_{g1} - \dot{\phi}(t) + S_1(t) & 0 & \frac{1}{2}\Omega_{e1}(t) \\ \frac{1}{2}\Omega_{g2}(t) & 0 & \Delta_{g2} - \dot{\phi}(t) + S_2(t) & \frac{1}{2}\Omega_{e2}(t) \\ \Omega_{ge}(t) & \frac{1}{2}\Omega_{e1}(t) & \frac{1}{2}\Omega_{e2}(t) & -2\dot{\phi}(t) + S_e(t) - i\frac{1}{2}\Gamma_e(t) \end{bmatrix}. \tag{A11}$$

However, we have checked numerically that the two-state model is still a good approximation for peak intensities up to $I = 10\ \mathrm{GW/cm^2}$, in particular, due to the additional Stark shift S_2 that allows state 2 to be sufficiently shifted from the resonance.

APPENDIX B: SPECTROGRAM FOR TWO-PHOTON PROCESSES

To provide an intuitive picture of the time evolution of the spectrum of the laser, timefrequency spectrograms such as the Wigner function have been proposed (see, for instance, Refs. [32,33]). The Wigner function of an electric field $E(t)$ can be written as [32]

$$W(\omega,t) = \int E^*(\omega + \omega'/2)E(\omega - \omega'/2)\, e^{i\omega t}\, d\omega'. \tag{B1}$$

For a two-photon process, we prefer to use a second-harmonic Wigner function defined as

$$W_2(\omega,t) = \int W(\omega',t)W(\omega - \omega',t)\, d\omega'. \tag{B2}$$

The absolute value of this second-harmonic Wigner function defines the two-photon spectrogram used in Figs. 1, 3, and 4.

[1] A. M. Weiner, Rev. Sci. Instrum. **71**, 1929 (2000).
[2] M. Shapiro and P. Brumer, *Principles of the Quantum Control of Molecular Processes* (Wiley, New York, 2003).
[3] D. J. Tanner and S. A. Rice, J. Chem. Phys. **83**, 5013 (1985).
[4] R. S. Judson and H. Rabitz, Phys. Rev. Lett. **68**, 1500 (1992).
[5] Z. Zheng and A. M. Weiner, Chem. Phys. **267**, 161 (2001).
[6] T. Hornung, R. Meier, D. Zeidler, K.-L. Kompa, D. Proch, and M. Motzkus, Appl. Phys. B **71**, 277 (2000).
[7] S. Guérin, S. Thomas, and H. R. Jauslin, Phys. Rev. A **65**, 023409 (2002).
[8] T. C. Weinacht, J. Ahn, and P. H. Bucksbaum, Nature (London) **397**, 233 (1999).
[9] A. Monmayrant, B. Chatel, and B. Girard, Phys. Rev. Lett. **96**, 103002 (2006).
[10] N. Dudovich, D. Oron, and Y. Silberberg, Nature (London) **418**, 512 (2002).
[11] D. Meshulach and Y. Silberberg, Nature (London) **396**, 239 (1998).
[12] N. Dudovich, B. Dayan, S. M. Gallagher Faeder, and Y. Silberberg, Phys. Rev. Lett. **86**, 47 (2001).
[13] N. Dudovich, D. Oron, and Y. Silberberg, Phys. Rev. Lett. **92**, 103003 (2004).
[14] M. C. Stowe, A. Pe'er, and J. Ye, Phys. Rev. Lett. **100**, 203001 (2008).
[15] N. P. Garayantz, V. S. Grigoryan, S. A. Michaelian, K. B. Petrossian, and K. M. Pokhsrarian, J. Mod. Opt. **38**, 591 (1991).
[16] N. Dudovich, T. Polack, A. Pe'er, and Y. Silberberg, Phys. Rev. Lett. **94**, 083002 (2005).
[17] M. Wollenhaupt, A. Präkelt, C. Sarpe-Tudoran, D. Liese, and T. Baumert, Appl. Phys. B **82**, 183 (2006).
[18] C. Trallero-Herrero, J. L. Cohen, and T. Weinacht, Phys. Rev. Lett. **96**, 063603 (2006).
[19] H. Suchowski, A. Natan, B. D. Bruner, and Y. Silberberg, J. Phys. B **41**, 074008 (2008).
[20] E. A. Shapiro, V. Milner, C. Menzel-Jones, and M. Shapiro, Phys. Rev. Lett. **99**, 033002 (2007).
[21] S. Guérin and H. R. Jauslin, Adv. Chem. Phys. **125**, 147 (2003).
[22] S. Lee, J. Lim, and J. Ahn, Opt. Express **17**, 7648 (2009).
[23] U. Boscain, G. Charlot, J.-P. Gauthier, S. Guérin, and H. R. Jauslin, J. Math. Phys. **43**, 2107 (2002).
[24] C. Trallero-Herrero, D. Cardoza, T. C. Weinacht, and J. L. Cohen, Phys. Rev. A **71**, 013423 (2005).
[25] J. Marek, Phys. Lett. A **60**, 190 (1977).
[26] B. H. Bransden and C. J. Joachin, *Physics of Atoms and Molecules*, 2nd ed. (Prentice Hall, Harlow, 2003).
[27] B. Broers, H. B. van Linden van den Heuvell, and L. D. Noordam, Phys. Rev. Lett. **69**, 2062 (1992); P. Balling, D. J. Maas, and L. D. Noordam, Phys. Rev. A **50**, 4276 (1994).
[28] A. Sieradzan, M. D. Havey, and M. S. Safronova, Phys. Rev. A **69**, 022502 (2004).
[29] G. Simons, J. Chem. Phys. **55**, 756 (1971).
[30] I. L. Glukhov and V. D. Ovsiannikov, J. Phys. B **42**, 075001 (2009).
[31] L. P. Yatsenko, T. Halfmann, B. W. Shore, and K. Bergmann, Phys. Rev. A **59**, 2926 (1999).
[32] J. Paye, IEEE J. Quantum Electron. **28**, 2262 (1992).
[33] A. Monmayrant, S. Weber, and B. Chatel, J. Phys. B **43**, 103001 (2010).